Site-Selective Atomic Layer Deposition on Rutile TiO2: Selective Hydration as a Route to Target Point Defects

Journal:	*The Journal of Physical Chemistry*
Manuscript ID	jp-2022-06992v.R1
Manuscript Type:	Article
Date Submitted by the Author:	08-Dec-2022
Complete List of Authors:	Kamphaus, Ethan; Argonne National Laboratory, Jones, Jessica; Argonne National Laboratory Shan, Nannan ; Argonne National Laboratory, Materials Science Martinson, Alex; Argonne National Laboratory, Materials Science Division Cheng, Lei; Argonne National Laroratory, Materials Science Division

Site-Selective Atomic Layer Deposition on Rutile TiO_2: Selective Hydration as a Route to Target Point Defects

Ethan P. Kamphaus[1], Jessica Catharine Jones[1], Nannan Shan[1], Alex B. F. Martinson,[1], Lei Cheng[1],**

[1]Materials Science Division, Argonne National Laboratory, Lemont, IL, 60439, USA

Keywords: ALD, r-TiO_2, DFT, nucleation, point defects, site selective, surface chemistry

ABSTRACT

Routes to area- and especially site-selective atomic layer deposition (ALD) remain an enticing challenge in precision surface science, despite the potentially game-changing capability for many energy applications. An unparalleled level of surface reaction control is required to direct ALD to select sites on the same nominal material, for example, targeted growth on distinct phases, facets, step-edges, and/or defects. However, as a sequential surface synthesis method ALD is uniquely suited to these challenges, including the possibility of selective deposition at defective surface atom arrangements. We computationally identify conditions for site-selective ALD through hydration of surface defects, including oxygen vacancies and titanium interstitials on low-index rutile TiO_2 facets. First-principles computation is used to predict, as a function of temperature, the hydroxylation of defects that are targeted by proton-exchange meditated ALD processes. In situ ellipsometric measurements of ALD Al_2O_3 nucleation on TiO_2 (110) single crystals prepared with and without abundant oxygen vacancies demonstrates striking contrast, corroborating computational predictions and revealing a mechanistically clear path to site-selective ALD.

INTRODUCTION

In the field of microfabrication, atomic layer deposition (ALD) has been a pivotal technology for nanoscale growth of metal oxides[1, 2]. Since it was first proposed in the 1960-1970s, the technique has enabled thin film growth with exquisite conformality and thickness control for an ever growing list of materials[3]. The unique capabilities of ALD arise from the self-limiting and sequential surface reactions[4]. The most ubiquitous of these reactions is the synthesis of Al_2O_3 via alternating reaction of trimethylaluminum (TMA) with a hydroxylated surface and subsequent reaction of water with the resulting aluminum-methylated surface in order to regenerate a freshly hydroxylated surface[5, 6]. Alternating these complementary TMA and H_2O surface reactions allows for thin film growth with sub-monolayer thickness control. Myriad complementary surface chemistries have been identified that enable the ALD of elemental metal, oxide, sulfide, and fluoride films across the periodic table[2, 7]. Recent efforts have focused on area-selective ALD in which the chemical specificity of volatile precursor reactivity can be leveraged to strongly favor nucleation on one material surface over another[8-10]. Area-selective ALD patterning allows for bottom-up synthesis of multiple materials without the need for mask alignment and with less material waste. An even greater level of surface reaction control is required to direct ALD to select sites on the same nominal material, for example, targeted growth on distinct phases, facets, step-edges, and/or defects. While uniquely challenging, site-selective ALD may allow exquisite control of surface passivation, defect amelioration, or facet-specific catalysis. The first challenge of site-selective ALD is to identify a strategy by which selective surface chemical control may be exerted over the heterogeneous surface. We recently identified a site-selective hydration strategy that leverages computationally predicted differences in the thermodynamic stability of water and surface hydroxyl at some step edge sites vs terraces of low-index rutile TiO_2 and In_2O_3.[11,12]

Exposure of a selectively hydrated surface to a volatile metalorganic precursor that is reactive only through proton exchange should result in nucleation specific to hydrated/hydroxylated sites. The selective hydration approach offers a straightforward method to direct ALD reactions to specific sites if sufficiently large differences in the site-dependent hydration process conditions exist among the surface sites of interest.

Rutile TiO_2 surfaces are known to exhibit point defects, including oxygen vacancies[13-23] and titanium interstitials[20-22, 24-27], the concentration of which depends on the surface preparation conditions. As point defects exhibit significantly different coordination environments relative to pristine terrace sites, these sites may also offer distinct hydration behavior. Therefore, we hypothesize that while the distinct atomic arrangements of point defects produce heterogeneous electronic states that may obscure strict structure-function relationships, their unique surface chemistry may offer the opportunity to selectively address and ameliorate these defects via site-selective ALD.

The presence of point defects in rutile TiO_2 has been studied with computation and simulations through direct calculation of the formation energy for both bulk[21, 28] and surface configurations[29, 30]. These studies predict which vacancies and interstitials are expected to occur at distinct experimental conditions, including temperature, partial pressure of oxygen gas, and electrochemical bias. Rutile TiO_2 surface oxygen vacancy (v_O'') and Ti interstitial (Ti_i'''') point defects have been examined with both computation and experimental investigations for a variety of adsorbate chemistries[17]. Previous reports have predicted the electronic structure of point defects with multiple levels of theory[18, 22]. Others have examined CO oxidation by incorporating both oxygen vacancies and titanium interstitials in order to demonstrate the pivotal role that defects play in catalytic applications[20]. For example, the presence of titanium interstitials assists with the

dissociation of adsorbed O_2 species on the rutile TiO_2 surface. Investigations into H_2O adsorption behavior have also been carried out with both experiment[26, 27] and simulation[31, 32]. However, despite the prevalence of previous research in this area, the information required to evaluate selective hydration is notably missing.

We use first principles simulation methods to accurately determine the water adsorption free energies on the (110), (100), (101) and (001) facets in order to identify conditions under which oxygen vacancies and titanium interstitials can be selectively targeted with ALD via a selective hydration strategy. The computational predictions guide experiments that reveal dramatically different nucleation rates on TiO_2 (110) facets with disparate surface point defect populations, consistent with the computational prediction of site-selective ALD.

METHODS

First-principles computational simulations in the form of density functional theory (DFT) must be carried out for comparisons to the previous work. However, "plain" DFT such as a general gradient approximation (GGA) functional used in our previous work to study non-defective surfaces is known to have shortcomings for simulating systems with *d* or *f* electrons such as rutile TiO_2 with defects[18, 33]. Specifically, this method is known to overestimate electronic delocalization and thus metallic behavior due to not appropriately canceling the coulombic self-interaction[34-37]. This has the effect of underestimating bandgaps, and potentially modifying energetics as well as other results in the system[38]. The tendency of GGA-DFT to favor delocalization is an assumption that introduces some errors but is considered to be acceptable in many systems. For the study of metal oxides such as TiO_2, the effect may be pronounced due to the *d* orbitals in the valence of the system[33]. Additionally, defects have a localized electron cloud that can be delocalized by GGA-DFT[18, 39, 40].

One straightforward approach to mitigating this problem is to incorporate some degree of exact exchange via hybrid DFT functionals such as B3LYP or B3PW91[41-43]. These methods, which are also popular for simulating molecules, do not suffer the same delocalization of electron density but are significantly more computationally expensive in a plane wave basis. Inherently, DFT does not contain exact exchange since the mathematical description of the exchange energy is within the exchange-correlation functional (which is not known exactly)[44]. Hybrid DFT uses a wavefunction approach in addition to the electron density approach so that the exchange may be calculated exactly. Unfortunately, this takes away the computational speed advantage of DFT versus other methods and makes larger simulations at this level of theory impracticable for most studies[45]. Another approach is the DFT+U method which is much less computationally expensive but requires an empirical parameter that must be closely fit for every unique system[36]. In DFT+U an additional term is added to the functional, which incorporates an on-site Coulomb repulsion on particular orbitals and atoms[46]. This allows for a simple scheme by which the self-interaction error and delocalization of orbitals are corrected for without losing the computational efficiency and performance of GGA-DFT[47]. The U parameter is determined by fitting the U to a certain electronic behavior in a material[48].

Both hybrid functional and DFT+U have been utilized various times for simulating the defects within rutile TiO_2.[18, 49, 50] Kowalski et al. offer a detailed look into simulations of defect formation energy on the (110) facet while rigorously comparing the differences between GGA-DFT, hybrid DFT and DFT+U.[32] They conclude that the differences in formation energy of vacancies among the methods are small, within ~0.3 eV in the largest difference. The same conclusions is echoed by Shi et al. where they found that "*results indicate that the values of adsorption energy are not obviously changed whether or not the U parameter is set"* in their study on bridging-oxygen

vacancies[50]. This surprising result demonstrates that despite the problems with GGA-DFT, this method is still able to accurately estimate the thermodynamics and equilibrium behavior of systems. Similar studies have been carried out for the titanium interstitial point defect as well both with and without the use of DFT+U[19, 51]. Kremer et al found that "*the energetics of the system is not qualitatively modified by the choice of U*" which shows that in both point defects that we have examined, DFT+U has been shown to have a minimal effect on the energetics. In addition to this vital conclusion, it is important to note that the energetics calculated within one level of theory are not comparable with another. By using hybrid DFT or DFT+U, the calculation method changes in a way that makes it not possible (or at least very inaccurate) to compare absolute energies. For these two reasons, we decided to utilize GGA-DFT for comparison to our previous study and in order to evaluate selective hydration.

GGA-DFT simulations were implemented within VASP utilizing the Perdew-Burke-Ernzerhof (PBE) exchange-correlation function with projector augmented wave pseudopotentials[52-56]. Consistent with our previous study, in all calculations, an electronic convergence energy of 1e-6 eV was used in addition to the Gaussian smearing parameter of 0.5 eV. Based on calculations done in previous work, the cutoff energy was selected to be 400 eV with a Gamma Centered K-point grid of 3x3x3[11]. Both the oxygen vacancy and titanium interstitial systems were created based on the literature discussed previously building on our previous asymmetric slab models where the bottom several layers of the slab are frozen to create a more surface like description. Similar construction methods, sizes and structures were utilized[28, 30]. All snapshots of structures in this work were obtained with OVITO.[57]

Single-side polished rutile TiO_2 single crystals with (110) orientation were obtained from MTI Corp and cleaned with an HF dip followed by DI water rinse. In order to remove organic

contaminants, improve terracing, and minimize v_O'''s the crystals were heated to 900 °C in air with a 5 °C/min ramp rate held at the set point temperature for 1 hr before cutting heating power to allow sample cooling at the natural rate of the tube furnace in a 1" quartz tube furnace (Lindberg/Blue M Mini-Mite). ALD processing and high vacuum annealing to produce v_O'''s was performed in a custom-built ALD tool, see SI for details. A dosing schedule of 1 s dimethylaluminum isopropoxide (DMAI), 120 s purge, 0.2 s H_2O, followed by 300 s purge was repeated for each cycle. The dosing schedule was optimized to provide a nearly saturating surface reaction that maximized the aluminum oxide growth rate/cycle when grown on itself, see Figure S35 and S36. The thickness of the aluminum oxide deposition was characterized in situ via spectroscopic ellipsometry (JA Woollam Co, M-2000, 245 to 1000 nm).

RESULTS & DISCUSSION

Oxygen Vacancies

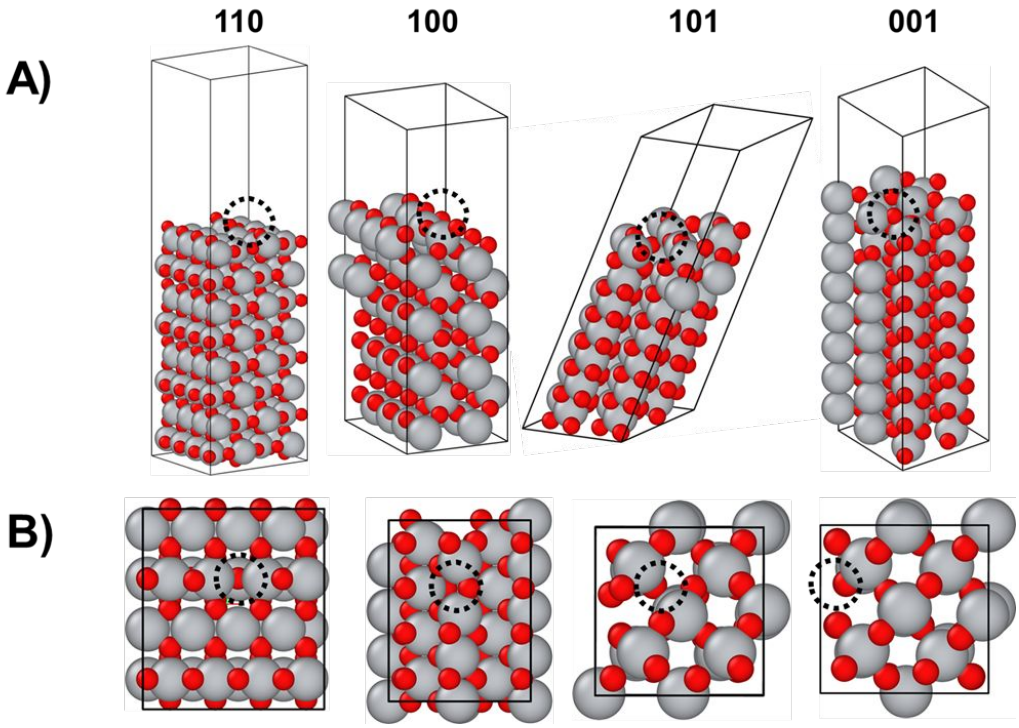

Figure 1. Oxygen vacancies for rutile TiO_2 for respective facets snapshots of A) whole system B) top-down view. Dotted circle shows location of v_O''.

Surface v_O'' models, shown in Figure 1, were constructed based on the rutile TiO_2 models used in our previous publication and in following previous studies on TiO_2 point defects[28, 30]. In each case, only one possible oxygen atom was considered for vacancy formation in each facet because there is only one symmetrically unique undercoordinated oxygen atom for each. Though it is possible that a fully coordinated but still exposed oxygen atom may also form vacancies, previous studies have identified these as energetically less favorable and therefore less likely to form. Depending on the surface preparation conditions, the defect surface concentration in the model may be higher than experimental values. However, achieving a small concentration in the model would require an impractically large simulation. For most experimental conditions, the experimental concentration will be lower than what is reasonably achievable in a DFT model. As long as the model is large enough that the defect is not interacting with itself across the periodic boundary conditions, then the energetics are representative of smaller concentrations. After the target oxygen atom is removed, the surface is optimized, resulting in structural rearrangement in every case. For the (110) facet, there is a mild perturbation in the Ti atoms where the vacancy is located but no significant rearrangement. On the (100) surface, an oxygen atom that was previously bonded to a subsurface Ti atom moves to a new position equidistant between its old position and that of the v_O''. v_O'' on (101) and (001) facets exhibit only mild perturbations similar to the (110) surface.

With the structures of surface oxygen vacancies obtained, molecular and dissociated water molecules were added to the surface to characterize their adsorption strength. There are multiple possible sites where water could adsorb on the surface, including on Ti atoms next to the oxygen

vacancy as well as Ti atoms far from the defect. We have assumed that Ti atoms far from the defect will provide nearly the same result as a pristine terrace, so H_2O molecules were only placed near the defect. A comparison of the molecular and dissociated H_2O absorption energy on a pristine terrace versus v_O'' site for the (110) facet as a function of temperature reveals dramatically different thermodynamics, Figure 2.

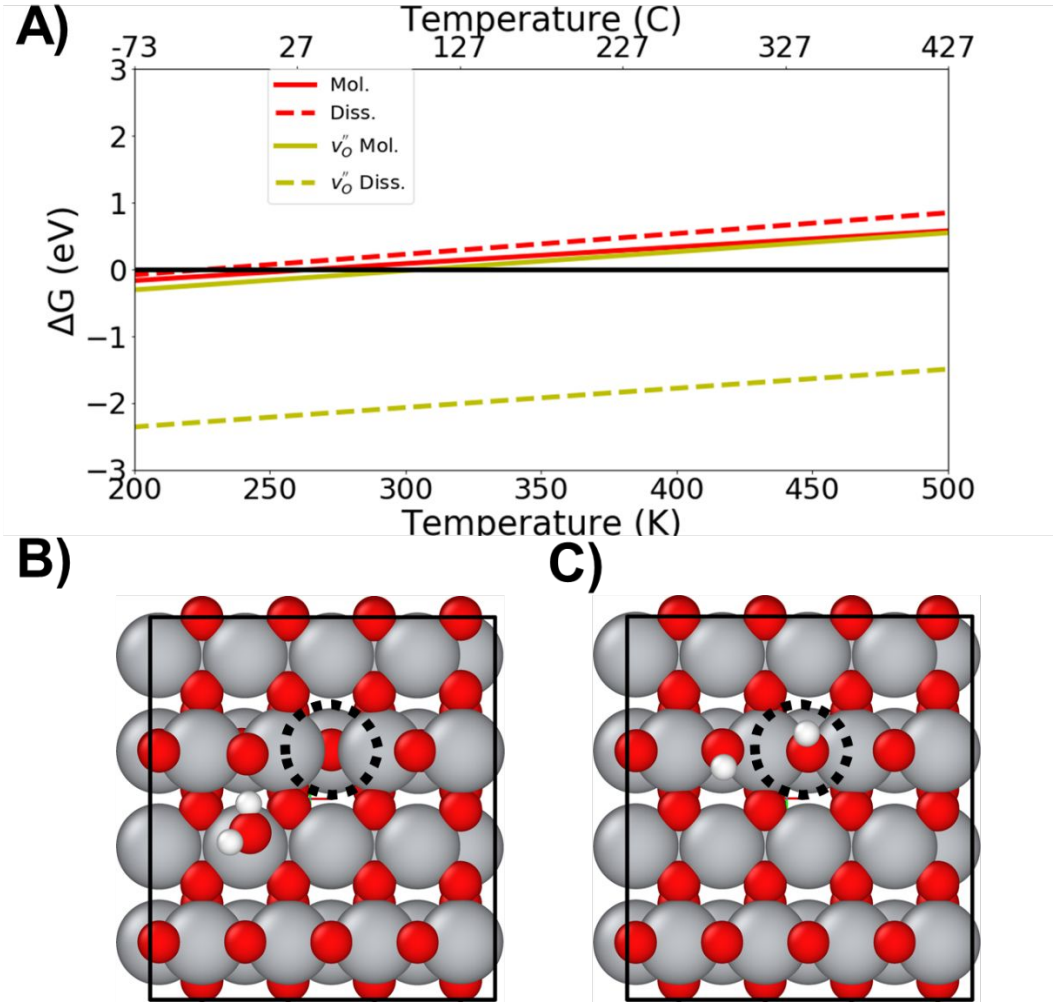

Figure 2. A) Free energy of molecular and dissociative H_2O adsorption at pristine terrace and surface v_O'' sites of TiO_2 (110) at 10 mTorr. B) top-down view of molecularly adsorbed H_2O near v_O'' . C) top-down view of dissociated H_2O near former v_O''. Dotted circle shows location of former v_O''.

The red curves representing the molecular and dissociated H_2O configurations on a pristine terrace are nearly overlapped and have a desorption temperature of ~ 250 K which were calculated in our previous work[11]. The solid yellow line represents the structure shown in Figure 2B, which had the initial structure of a molecular water adsorbed on the Ti atoms proximal to the v_O'' site. However, the final structure does not represent this; instead, the water molecule is adsorbed to a nearby Ti atom. This movement occurred during the simulation's optimization to obtain the lowest (and therefore equilibrium) structure, indicating that the system found a lower energy configuration by moving the water away from the vacancy as shown in Figure 2B. Despite the system's resistance to creating the molecular H_2O adsorption on the v_O'' , this offers insight into the extent to which the v_O'' influences adsorption on other sites. Since the lines essentially overlap, it is clear that the Ti atoms that are not directly adjacent to the v_O'' are not significantly influenced. In contrast to the previous three water binding sites and modes, H_2O readily adsorbs at the v_O'' site and replaces the missing oxygen atom in the surface structure. Dissociated H_2O adsorption exhibits a much larger adsorption strength with desorption temperature over 700 K. As discussed in our previous work, the interaction between H_2O and the (110) surface of r-TiO_2 is a well-studied system[11]. However, the exact conditions of each study make it difficult to compare results readily especially when considering the free energy which is not as commonly reported and other variables such as pressure, surface coverage and other geometries such as oxygen vacancies near steps and etc. For the surface coverage in particular, we expect that higher coverages will introduce favorable interactions between adsorbed water molecules on the surface. However, for evaluating selective hydration we are concerned with the limited case which represents when the first/last molecule adsorbed to the surface. In addition the results shown in Figure 2 are in line with previous studies

of H_2O adsorbing on oxygen vacancies due to the increased strength of adsorption relative to the pristine terrace[32].

The remaining low-index facets exhibit hydration energies that are distinct from the (110) facet, Figure 3.

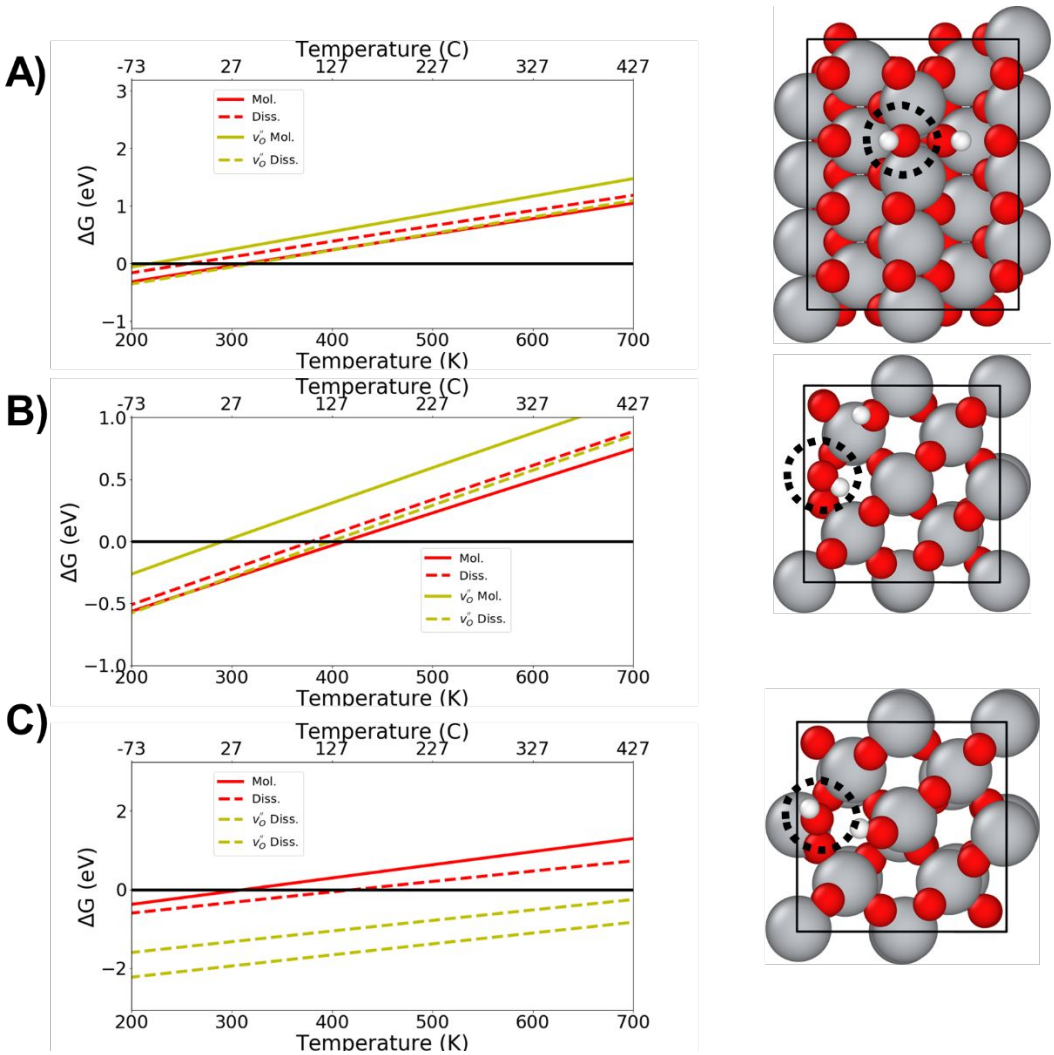

Figure 3. Free energy of molecular and dissociative H_2O adsorption at pristine terrace and surface VO and top-down view of most favorable adsorbed H_2O near v_O'' for A) (100) B) (101) C) (001) facets at 10 mTorr. Dotted circle shows former location of v_O''

On the (100) facet, the dissociated case is favored at the v_O'' and the OH fragment replaces the vacancy in the structure just as in the (110). However, this configuration does not offer a large

increase in adsorption strength over the pristine terrace. In the pristine terrace model, the desorption temperature for dissociated water is ~300 K versus ~325 K for the v_O'' model, which demonstrates a much smaller difference compared to the (110) facet. In the (101) model, the dissociated configuration was also favored, however, the resulting free energy of adsorption is nearly identical to that on a pristine terrace surface. On rutile TiO_2 (001), the molecular input configuration was also energetically favorable but the resulting structure is clearly dissociated. This is another example of the configuration changing more than expected, similar to the (110) molecular water adsorption moving away from the v_O''. Whether the initial structure was molecular or not, the outcome of the simulation favored dissociation and with a significant increase in adsorption strength relative to the adsorption strength of H_2O in the most stable pristine terrace configuration.

In all low-index facets, the dissociative adsorption of H_2O is favored, which is not the case for pristine terraced facets. We hypothesize that dissociative adsorption is favored due to the ability of an OH fragment to fill the vacant oxygen site on the surface, while in the molecular configurations, the H_2O molecules are never located in place of the vacancy but only adjacent to it. As for the variety of adsorption free energies, there is no clear pattern in atom arrangement that can be tied to a particular feature, in the same way that step edge atom arrangements on different facets do not exhibit the same H_2O adsorption free energies, as noted in the previous study[11].

Though we do not evaluate the interaction of a metalorganic precursor such as TMA with the hydroxylated surface, the reaction between TMA and adsorbed H_2O or OH species is known to be highly exothermic[58-60]. This indicates that as long as the surface is hydrated, then the subsequent reaction will occur because of the large downhill move in overall energy from the favorable reaction.

The selective hydration strategy for site-selectivity ALD requires that proton-exchange reactions are the only viable surface reaction. For example, the direct reaction of the metalorganic ALD precursors with pristine terrace sites could provide a route to unselective growth. This is an important but challenging caveat, as every metalorganic ALD precursor of interest needs be individually screened for potential reaction at every distinct surface site of interest for every facet. We previously predicted the absorption of TMA to be favorable at temperatures below 275 C for all low-index rutile TiO_2 facet terraces with the exception of (100), indicating that less reactive metalorganic ALD precursors should be considered[11]. However, the direct reaction of a metalorganic ALD precursor *exclusively* with defect sites could also provide an alternative pathway to site selectivity. We investigate one such case here where TMA is chosen as a highly reactive and ubiquitous ALD precursor, Figure 4.

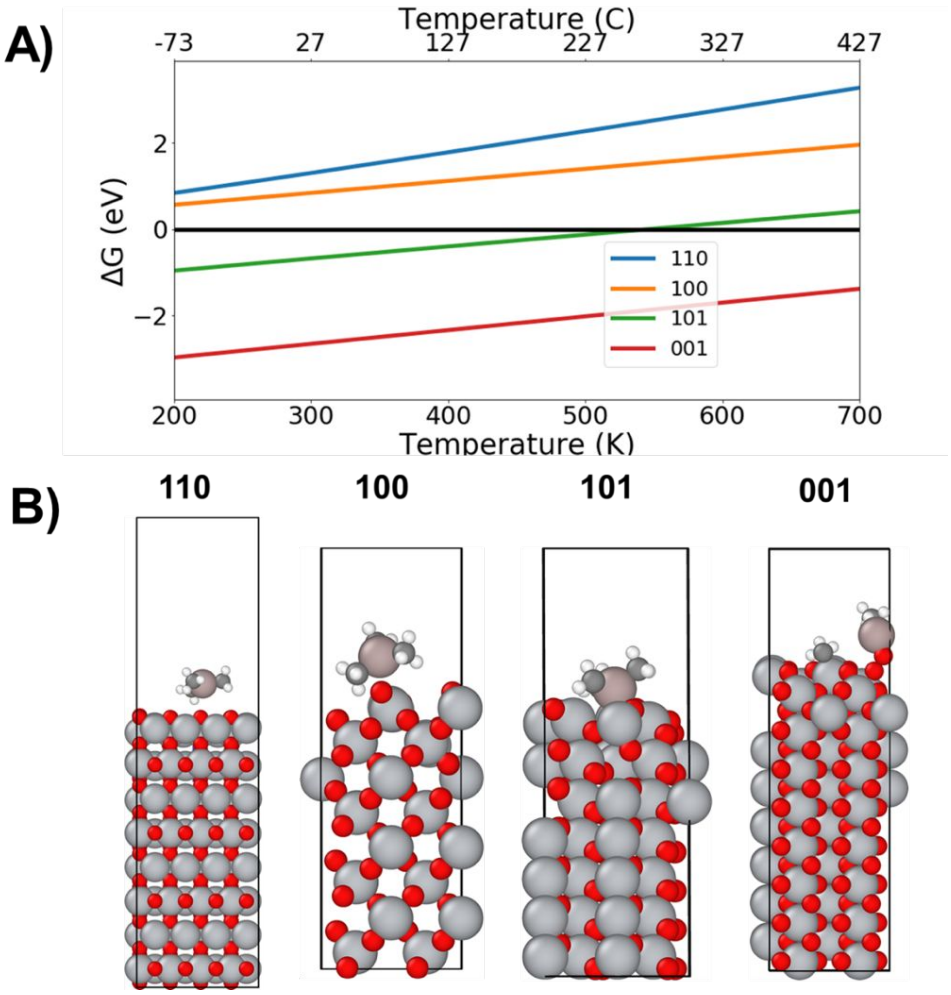

Figure 4. A) Free energy of adsorption of TMA on v_O'' at 10 mTorr. B) Snapshots of optimized structures.

Thermodynamically favorable adsorption is predicted at v_O'' for the (101) and (001) facets at typical ALD temperatures below ~270 °C. However, TMA absorption on (110) and (100) is unfavorable for all temperatures greater than room temperature. The main difference between the optimized TMA absorption structures is the distance between the TMA and the surface. In the (110) and (100) models, the TMA approaches the surface to weakly interact with the v_O'', while in the case of the (101) and (001) facets the TMA is chemisorbed to a surface oxygen atom. The combination of surface configuration as well as the energetics of the system cause the TMA to

have closer interaction with those facets, which is reflected in the free energy of adsorption. Therefore, we predict the opportunity for site-selective growth at v_O'' absorption on both (001) and (101) facets through direct metalorganic reactions. As with the hydrated surface, if an adsorbed TMA species is exposed to gas phase H_2O, the species are expected to react due to their highly exothermic reaction chemistry[58]. Even if the interaction energy of TMA on the surface is not very low, it will be energetically favorable for the reaction to occur..

Titanium Interstitials

Models for Ti_i'''' were constructed with a procedure similar to that described for the oxygen vacancies. There are few symmetrically unique locations for a Ti_i'''' to occur on the surface, which greatly reduces the state space of configurations for each facet. In the (110), (101), and (001) models, Figure 5, the resulting Ti_i'''' atom has a coordination of 3 with oxygen atoms and causes minimal rearrangement to the surface. On the (100) facet, the Ti on the surface has a coordination of 4 because one of the undercoordinated oxygen atoms on the surface rearranges to coordinate with the addition of the Ti atom.

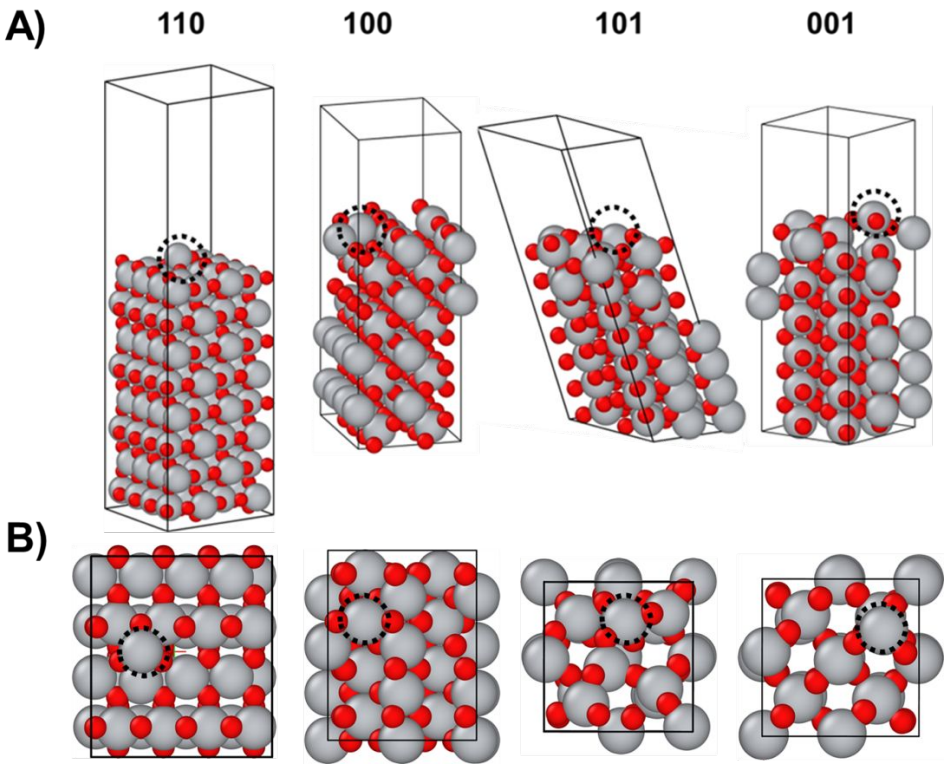

Figure 5. Ti_i'''' for rutile TiO_2 for respective facet snapshots of A) whole system B) top-down view. Dotted circle shows location of i_{Ti}.

Titanium interstitial models were constructed with a procedure similar to that described for the oxygen vacancies. There are few symmetrically unique locations for a Ti interstitial to occur on the surface, which greatly reduces the state space of configurations for each facet. Each model that was used for further simulations is displayed in Figure 5. In the (110), (101), and (001) models, the resulting interstitial Ti atom has a coordination of 3 with oxygen atoms and causes minimal rearrangement to the surface. On the (100) facet, the Ti on the surface has a coordination of 4 because one of the undercoordinated oxygen atoms on the surface rearranges to coordinate with the addition of the Ti atom.

As in the V_O simulation, the potential for selective hydration was tested by adding water molecules to the point defect in both the molecular and dissociated configurations. In the (110),

(100), and (101) facets, the dissociative H_2O adsorption is energetically favorable relative to pristine surface sites, Figure 6. In all models, the molecular configuration is located on the Ti_i'''' and the dissociated cases have an OH on the defect with a nearby H atom.

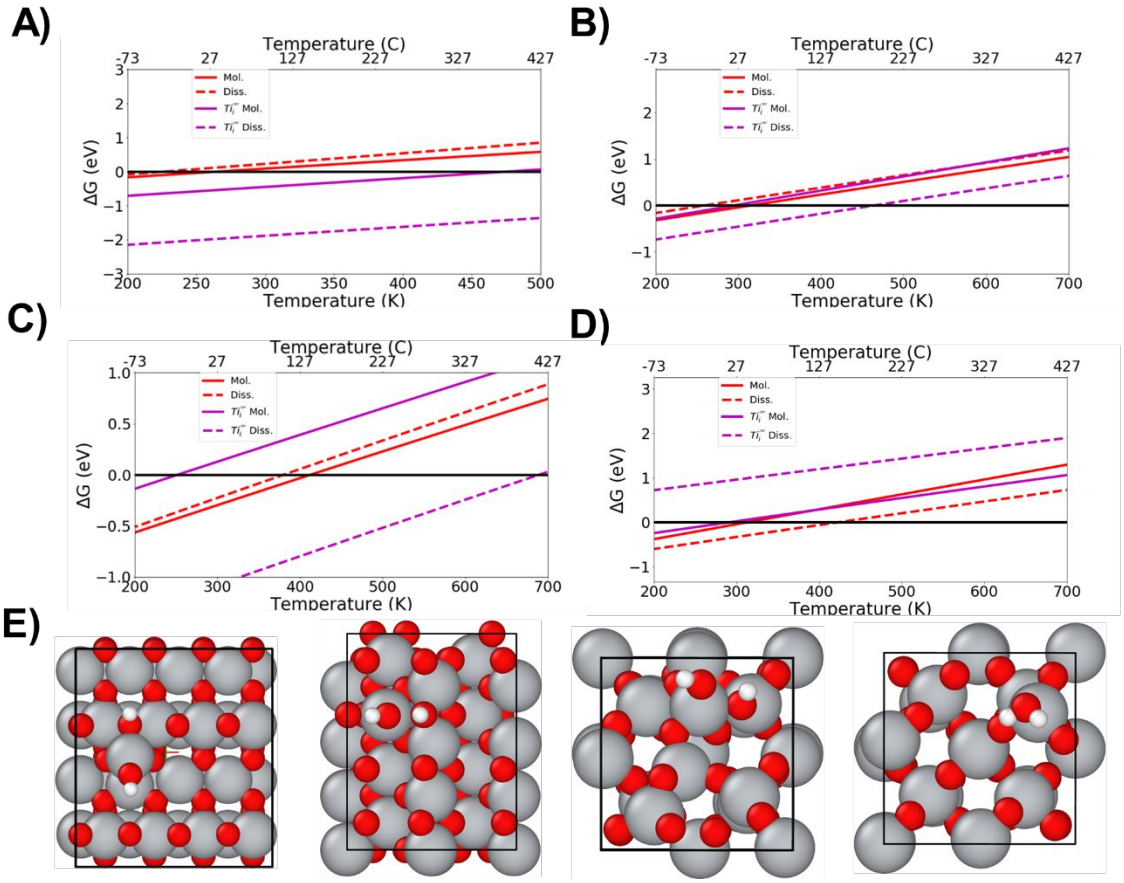

Figure 6. Adsorption of H_2O on Ti interstitial compared to pristine terrace for facets A) (110) B) (100) C) (101) D) (001) at 10 mTorr. and E)snapshots of most favorable H_2O adsorption on Ti_i''''

Molecular absorption configurations exhibit either similar energetics to the pristine surface or are less stable, demonstrating the unique electronic environment on/near the Ti_i''''. Interestingly, the (001) surface shows a significantly different behavior where H_2O adsorption on the Ti_i'''' is less stable than on the pristine surface. After examining the adsorption structures of the (001) versus the other facets, we find no clear difference that would indicate a change in trend. This suggests

that the explanations for the differences between facets arise from the subtle energetics of the Ti_i'''' and surface in each configuration as opposed to a more general, intuitive trend. The adsorption of TMA was not considered for the Ti interstitial defect because metalorganic precursors typically interact with oxygen sites as opposed to metal atoms. While there may be some small effect on the other oxygen sites due to the defect, the effect is likely small based on the earlier analysis of molecular H_2O adsorption on the (110) facet.

Selective Hydration

In the scheme for selective hydration, the selectivity arises from the favorability of the H_2O adsorption, which may be tuned with experimental conditions via selecting the growth temperature. If there is a sufficiently large difference between point defect and pristine terrace H_2O desorption temperatures, one may aim to hold the experimental condition at an intermediate temperature in order to selectively hydrate the site that requires greater desorption temperature. In the limit of exclusively proton-mediated surface reactions with the metalorganic ALD precursor, we hypothesize that metal deposition may be limited to *only those sites favored to remain hydrated at the selected experimental conditions*. With sufficiently unique hydration thermodynamics, temperature-controlled hydration may allow for selectivity among multiple unique sites on a single facet. In our previous work, we focused on selectivity for common step edges over the pristine terrace[11, 12]. With the additional consideration of point defects, we can now consider multiple temperature ranges over which various sites may be selectively hydrated. For example, the thermodynamic tipping points for (110) terrace, step, interstitial and vacancy hydration spans more than 600 degrees, Figure 7.

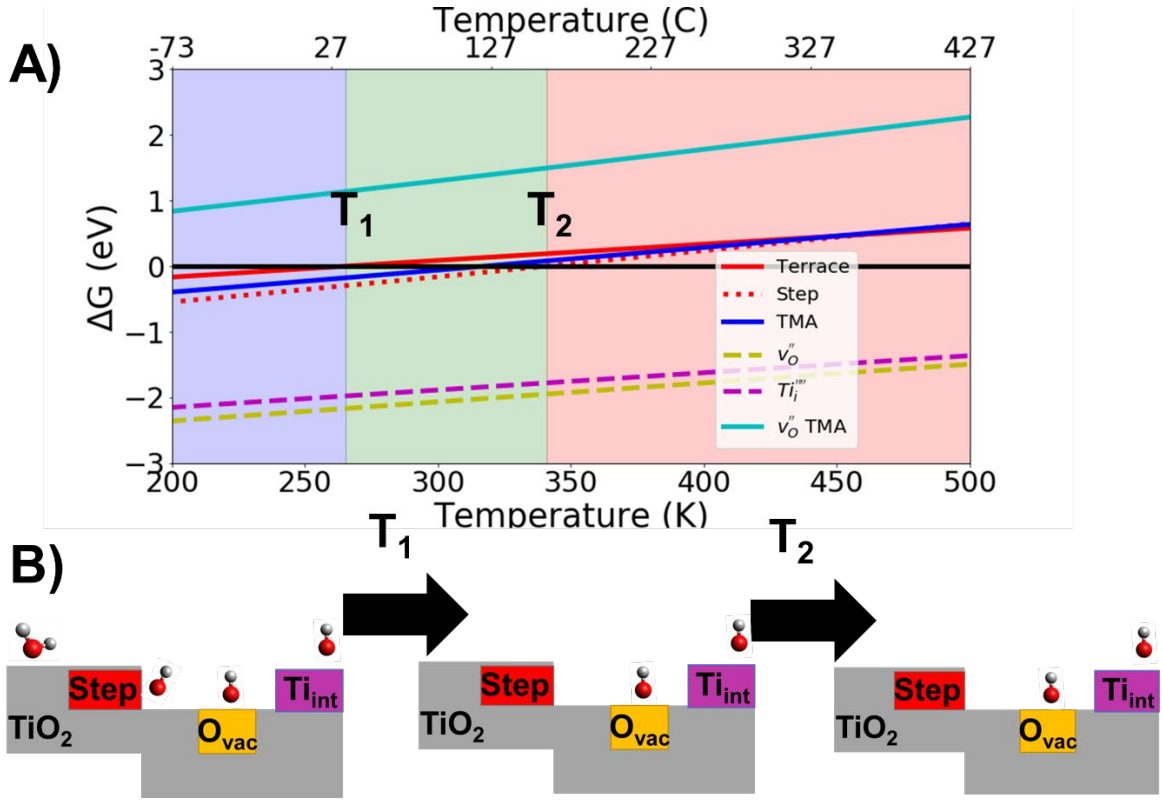

Figure 7. A) Free energy of adsorption comparison for (110) facet considering all sites examined in this work and previous. B) Illustration of how selectivity changes on the (110) facet as temperature changes.

For example, at temperatures slightly below T_1 (~265 K/blue), H_2O will remain adsorbed to all sites considered, including pristine terrace, step, and oxygen vacancies site. Above T_1 but less than T_2 (~265 to 350 K/green), the H_2O is predicted to desorb from the pristine terrace but will remain on the step, $v_{O,}''$ and i_{Ti} sites. For temperatures above T_2 (red), H_2O will only be adsorbed to such that deposition is expected exclusively at these sites. In the absence of V_O and Ti_i'''' sites, no deposition is predicted for temperatures above T_2. This temperature-tunable selectivity may offer unique control over which sites may be targeted by proton-exchange enabled ALD processes.

The previous analysis was repeated for the remaining low-index facets considered as shown in Figure 8.

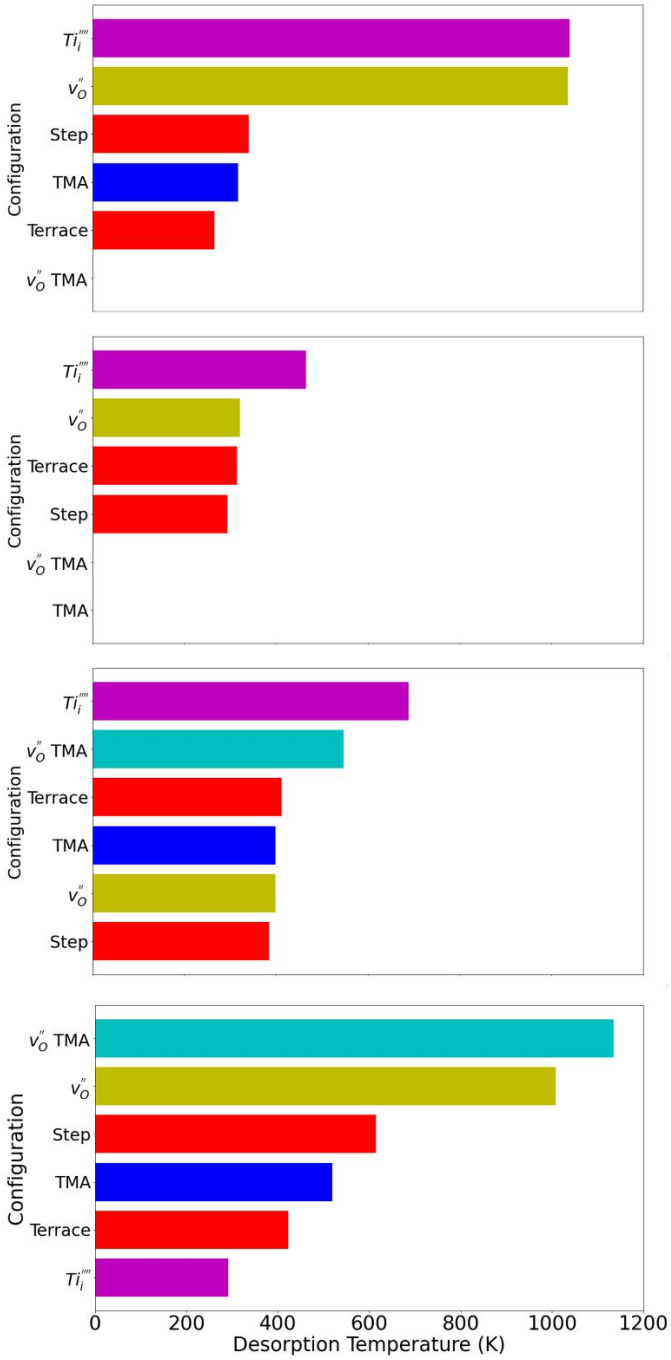

Figure 8. Desorption Temperatures of H_2O on different sites as for A) (110) B) (100) C) (101) and D) (001) facets at 10 mTorr. The corresponding data is listed in Table S-1.

Similar to the (110) facet, H_2O adsorption at v_O'' point defects is also strongly favored over pristine terrace sites on the (001) facet. However, H_2O adsorption on Ti_i'''' is also favored on the (110) facet. Therefore, the (110) surface can be thought of as fully defect selective at intermediate temperatures (~350 to >700 K). In the (100) model, the Ti interstitial has a 150 K greater desorption temperature than both the v_O'' and pristine terrace site. For the (101) facet the H_2O desorption at each distinct site is neatly separated by at least 100 K. TMA adsorption at the v_O'' also provides a pathway for selective growth as the precursor will react with H_2O in the next exposure cycle. In every facet, at least one of the defects offers selective hydration over the pristine facet.

The free energies for H_2O desorption have been predicted at a H_2O partial pressure of 10 mTorr, which approximates the experimental partial pressure during H_2O dosing. Though the pressure will have no influence on the DFT ground state structures and equilibrium, the pressure will change the $\Delta G_{adsorption}$ due to the change of free energy for the gaseous state. Exceeding dry and well purged ALD tools may achieve significantly lower H_2O partial pressures, influencing the desorption temperature. We also investigated how the free energy would change if the pressure was 1e-8 Torr instead. As expected, a lower H_2O partial pressure makes absorption less favorable, shifting desorption to lower temperature, Figure S1-5. The 6 orders of magnitude change in H_2O partial pressure induces a change of at least 100 K depending on the configuration in question. The H_2O desorption site order is retained but is likely to shift relative to the absorption of the metalorganic precursors, offering further tunability to the site-selective ALD approach.

Experimental Validation

The computational predictions for site-selective hydroxylation of rutile TiO_2 were experimentally tested via ALD on (110)-oriented single crystal substrates. The (110) surface was selected for the large difference (>700 °C) in predicted H_2O desorption temperature for terrace

versus v_O'' sites, see Figure 8. The (110) surface is also readily prepared to exhibit an atomically smooth terraced surface with relatively large (~100 nm) plateaus, Figure S33. Two nominally identical crystals were fired in air to 900 °C in order to favor terrace growth, remove potential organic surface contamination, and minimize the number of oxygen vacancies. The crystal is nearly colorless and exhibits >10 MOhm electrical resistance, indicating a low density of the v_O'' defect that leads to n-type doping. A nominally identical crystal was further annealed at 900 °C under high vacuum (~1e-7 Torr) for 1 hour in order to create a high density of v_O'' sites in the bulk and surface. The creation of v_O'''s is readily confirmed by the blue color of the TiO_2 single crystal, see Figure S44, as well as an electrical conductivity that is increased by more than 106 orders of magnitude. While both the blue color and bulk conductivity are consistent with v_O'''s in the bulk, a significant fraction of v_O'''s are also present on the surface[22, 61, 62].

An ALD process for Al_2O_3 using dimethylaluminum isoproxide (DMAI) and H_2O at 150 °C was selected to investigate site-selective growth. The mechanism for ALD growth was previously deduced from mass spectroscopic study to include proton-exchange of surface hydroxyl with methyl ligands to release methane.[63-65] We hypothesized that the lower reactivity of DMAI may allow greater selectivity for strictly proton-exchange reactions that require surface hydration/hydroxylation compared to the more common TMA precursor, for which additional surface reactions beyond proton-exchange have been predicted and demonstrated[58, 66-68]. A self-saturating ALD process for Al_2O_3 was established with saturating growth rate of ~1.0 Å/cycle, Figure S35-36, with in situ spectroscopic ellipsometry. An optimized ALD recipe was applied to nucleation and growth on a growing Al_2O_3 film front, a clean Si/SiO_2 surface, an oxidized TiO_2 (110) surface, and finally a vacuum annealed TiO_2 (110) with v_O'', Figure 9.

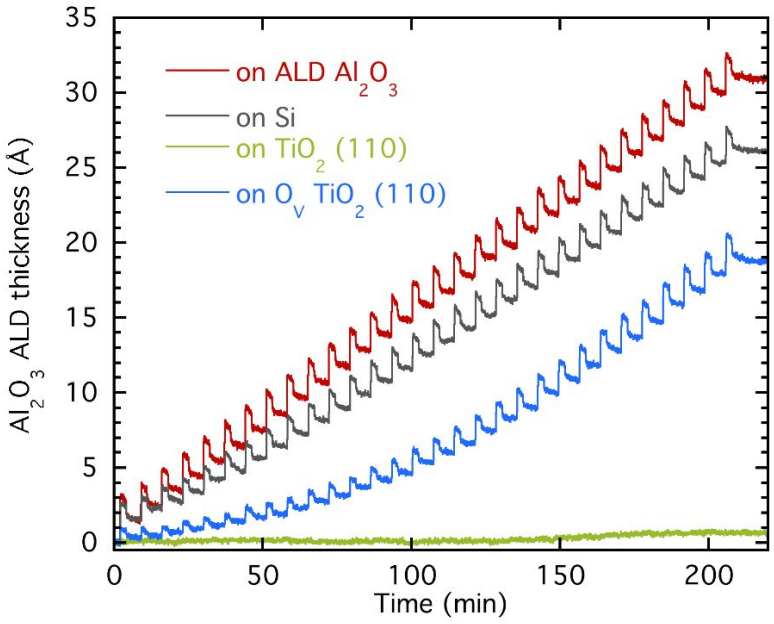

Figure 9. ALD Al_2O_3 film thickness on various substrates during 30 cycles of DMAI/H_2O growth at 150 C.

After nucleation has been established, the DMAI/H_2O process exhibits classic stair-step behavior with linear growth on itself corresponding to 1.03 Å/cycle. The densely hydroxylated SiO_2 surface presented by a Si substrate with native oxide at 150 °C induces only slight nucleation inhibited for ~10 cycles. In striking contrast, the nucleation and growth of Al_2O_3 on the terraced TiO_2(110) single crystal is nearly completely inhibited. The absence of growth is in remarkable agreement with the computational prediction of no growth on non-hydroxylated terrace and step sites at 423K. Examples of such complete inhibition of ALD growth are exceedingly rare, especially for metal oxide ALD on other metal oxides. This clear inhibition on terrace TiO_2(110) opens new possibilities for robust selectivity over other surface sites including v_O'''s on the same TiO_2(110) facet, which are predicted to hold onto dissociatively absorbed water until more than 800 °C. The same ALD process applied to TiO_2(110) single crystals with v_O'''s induced by high-temperature vacuum annealing reveals dramatically different nucleation and growth that is intermediate

between pristine terraced TiO_2(110) and a densely hydroxylated Si surface. An intermediate nucleation delay is consistent with the site-selective growth of Al_2O_3 on hydroxylated v_O'' (and potentially i_{Ti}) sites only. Subsequent growth on deposited Al_2O_3 islands increases until the islands presumably coalesce, leading to the same expected growth rate of this process on a growing Al_2O_3 film front (1.0 Å/cycle) after ~25 cycles. While microscopic confirmation of site-selective deposition will require further advanced characterization, the computational prediction and distinct nucleation behavior of the ALD Al_2O_3 process on TiO_2(110) single crystals with and without intentional V_O incorporation provides strong evidence for site-selective ALD.With both computation and experiment, we have proven the use of selective hydration for site selective ALD on some facets of the r-TiO2 system. This approach provides a straightforward technique for targeting important point defects but is currently limited to the intrisic interactions of H2O with each defect. However, our exploration of the larger variable space of site-selective absorption interactions has only begun. To date, we have identified only a handful of H2O-specific site selective ALD pathways, however we continue to broaden our investigations other small molecules for selective adsorption or dehydration with the potential to dramatically expand the number of materials and conditions for which site selective ALD may possible. CONCLUSIONS

Computationally predicting and experimentally realizing site-selective atomic layer deposition will provide new opportunities for interface design and optoelectronic property improvement. First-principles computational simulations of oxygen vacancies and titanium interstitials afford ground state equilibrium structures and subsequent free energies for hydration of these common point defects. The direct absorption of metalorganic precursors at point defects in the absence of favorable thermodynamics for absorption at pristine terrace sites was also identified as a route to site selective atomic layer deposition. For the selective hydration approach, we found that for every

low-index facet investigated, there is at least one point defect, either v_O'' or Ti_i'''', which has a stronger adsorption energy than the pristine terrace or step edge sites. Experimental investigation of TiO_2 (110) oriented single crystal showed unparalleled inhibition of an Al_2O_3 ALD process, consistent with predictions from first principles computation. Intentional incorporation of v_O'''s into a TiO_2 (110) oriented single allows for nucleation under identical growth conditions. As many oxide defect sites exhibit strong adsorption of water, a selective hydration strategy for site-selective growth may be generalizable to other metal oxides.

ASSOCIATED CONTENT

Supporting Information. SI.pdf is included free of charge. Document contains additional free energy of adsorption figures, orthographic projections of simulated structures ,and supporting information for experimental characterizations.

Author Information

*Alex B. F. Martinson: martinson@anl.gov

*Lei Cheng: leicheng@anl.gov

Acknowledgements

This work was supported by the U.S. Department of Energy, Office of Science, Basic Energy Sciences, Materials Science and Engineering Division. We gratefully acknowledge the computing resources provided on Bebop, a high-performance computing cluster operated by the Laboratory Computing Resource Center at Argonne National Laboratory.

REFERENCES

1. George, S. M., Atomic Layer Deposition: An Overview. *Chemical Reviews* **2010,** *110* (1), 111-131.

2. Johnson, R. W.; Hultqvist, A.; Bent, S. F., A Brief Review Of Atomic Layer Deposition: From Fundamentals To Applications. *Materials Today* **2014,** *17* (5), 236-246.

3. Puurunen, R. L., A Short History Of Atomic Layer Deposition: Tuomo Suntola's Atomic Layer Epitaxy. *Chemical Vapor Deposition* **2014,** *20* (10-11-12), 332-344.

4. Lu, J.; Elam, J. W.; Stair, P. C., Atomic Layer Deposition—Sequential Self-Limiting Surface Reactions For Advanced Catalyst "Bottom-Up" Synthesis. *Surface Science Reports* **2016,** *71* (2), 410-472.

5. Gosset, L.; Damlencourt, J.-F.; Renault, O.; Rouchon, D.; Holliger, P.; Ermolieff, A.; Trimaille, I.; Ganem, J.-J.; Martin, F.; Semeria, M.-N., Interface And Material Characterization Of Thin Al_2O_3 Layers Deposited By ALD Using TMA/H2O. *Journal of Non-Crystalline Solids* **2002,** *303* (1), 17-23.

6. Widjaja, Y.; Musgrave, C. B., Quantum Chemical Study Of The Mechanism Of Aluminum Oxide Atomic Layer Deposition. *Applied Physics Letters* **2002,** *80* (18), 3304-3306.

7. Bent, S. F., Organic Functionalization Of Group IV Semiconductor Surfaces: Principles, Examples, Applications, And Prospects. *Surface Science* **2002,** *500* (1-3), 879-903.

8. Chen, R.; Kim, H.; McIntyre, P. C.; Porter, D. W.; Bent, S. F., Achieving Area-Selective Atomic Layer Deposition On Patterned Substrates By Selective Surface Modification. *Applied Physics Letters* **2005,** *86* (19), 191910.

9. Bobb-Semple, D.; Nardi, K. L.; Draeger, N.; Hausmann, D. M.; Bent, S. F., Area-Selective Atomic Layer Deposition Assisted By Self-Assembled Monolayers: A Comparison Of Cu, Co, W, And Ru. *Chemistry of Materials* **2019,** *31* (5), 1635-1645.

10. Lee, H.-B.-R.; Bent, S. F., A Selective Toolbox For Nanofabrication. ACS Publications: 2020; Vol. 32, pp 3323-3324.

11. Kamphaus, E. P.; Shan, N.; Jones, J. C.; Martinson, A. B.; Cheng, L., Selective Hydration of Rutile TiO_2 as a Strategy for Site-Selective Atomic Layer Deposition. *ACS Applied Materials & Interfaces* **2022,** *14* (18), 21585-21595.

12. Shan, N.; Jones, J. C.; Luo, C.; Hock, A. S.; Martinson, A. B.; Cheng, L., Selective Hydroxylation Of In_2O_3 As A Route To Site-Selective Atomic Layer Deposition. *The Journal of Physical Chemistry C* **2022.**

13. Chung, Y.; Lo, W.; Somorjai, G., Low Energy Electron Diffraction And Electron Spectroscopy Studies Of The Clean (110) and (100) Titanium Dioxide (Rutile) Crystal Surfaces. *Surface Science* **1977,** *64* (2), 588-602.

14. Mayer, J.; Diebold, U.; Madey, T.; Garfunkel, E., Titanium And Reduced Titania Overlayers On Titanium Dioxide (110). *Journal of Electron Spectroscopy and Related Phenomena* **1995,** *73* (1), 1-11.

15. Lusvardi, V.; Barteau, M.; Chen, J. G.; Eng Jr, J.; Frühberger, B.; Teplyakov, A., An NEXAFS Investigation Of The Reduction And Reoxidation Of TiO_2 (001). *Surface Science* **1998,** *397* (1-3), 237-250.

16. Henderson, M. A., A Surface Perspective On Self-Diffusion In Rutile TiO_2. *Surface Science* **1999,** *419* (2-3), 174-187.

17. Pang, C. L.; Lindsay, R.; Thornton, G., Structure Of Clean And Adsorbate-Covered Single-Crystal Rutile TiO_2 Surfaces. *Chemical Reviews* **2013,** *113* (6), 3887-3948.

18. Stausholm-Møller, J.; Kristoffersen, H. H.; Hinnemann, B.; Madsen, G. K.; Hammer, B., DFT+ U Study Of Defects In Bulk Rutile TiO_2. *The Journal of Chemical Physics* **2010,** *133* (14), 144708.

19. Wendt, S.; Sprunger, P. T.; Lira, E.; Madsen, G. K.; Li, Z.; Hansen, J. Ø.; Matthiesen, J.; Blekinge-Rasmussen, A.; Lægsgaard, E.; Hammer, B., The role of interstitial sites in the Ti 3d defect state in the band gap of titania. *Science* **2008,** *320* (5884), 1755-1759.

20. Yu, Y.-Y.; Gong, X.-Q., CO Oxidation At Rutile TiO_2 (110): Role Of Oxygen Vacancies And Titanium Interstitials. *ACS Catalysis* **2015,** *5* (4), 2042-2050.

21. He, J.; Behera, R.; Finnis, M.; Li, X.; Dickey, E.; Phillpot, S.; Sinnott, S., Prediction Of High-Temperature Point Defect Formation In TiO_2 From Combined Ab Initio And Thermodynamic Calculations. *Acta Materialia* **2007,** *55* (13), 4325-4337.

22. Nowotny, M.; Bak, T.; Nowotny, J., Electrical Properties And Defect Chemistry Of TiO_2 Single Crystal. I. Electrical Conductivity. *The Journal of Physical Chemistry B* **2006,** *110* (33), 16270-16282.

23. Diebold, U., Structure And Properties Of TiO_2 Surfaces: A Brief Review. *Applied Physics A* **2003,** *76* (5), 681-687.

24. Finazzi, E.; Di Valentin, C.; Pacchioni, G., Nature Of Ti Interstitials In Reduced Bulk Anatase And utile TiO2. *The Journal of Physical Chemistry C* **2009,** *113* (9), 3382-3385.

25. Morita, K.; Shibuya, T.; Yasuoka, K., Stability Of Excess Electrons Introduced By Ti Interstitial In Rutile TiO_2 (110) Surface. *The Journal of Physical Chemistry C* **2017,** *121* (3), 1602-1607.

26. Zhang, Z.; Lee, J.; Yates Jr, J. T.; Bechstein, R.; Lira, E.; Hansen, J. Ø.; Wendt, S.; Besenbacher, F., Unraveling The Diffusion Of Bulk Ti Interstitials In Rutile TiO_2 (110) By Monitoring Their Reaction With O Adatoms. *The Journal of Physical Chemistry C* **2010,** *114* (7), 3059-3062.

27. Lira, E.; Hansen, J. Ø.; Huo, P.; Bechstein, R.; Galliker, P.; Lægsgaard, E.; Hammer, B.; Wendt, S.; Besenbacher, F., Dissociative And Molecular Oxygen Chemisorption Channels On Reduced Rutile TiO_2 (110): An STM And TPD Study. *Surface Science* **2010,** *604* (21-22), 1945-1960.

28. Bjørheim, T. S.; Kuwabara, A.; Norby, T., Defect Chemistry Of Rutile TiO2 From First Principles Calculations. *The Journal of Physical Chemistry C* **2013,** *117* (11), 5919-5930.

29. Pabisiak, T.; Kiejna, A., Energetics Of Oxygen Vacancies At Rutile TiO2 (110) Surface. *Solid State Communications* **2007,** *144* (7-8), 324-328.

30. Bjørheim, T. S.; Kuwabara, A.; Mohn, C. E.; Norby, T., Defects At The (110) Surface Of Rutile TiO2 From Ab Initio Calculations. *International Journal Of Hydrogen Energy* **2012,** *37* (9), 8110-8117.

31. Wang, H.-L.; Hu, Z.-P.; Li, H., Dissociation Of Liquid Water On Defective Rutile TiO_2 (110) Surfaces Using Ab initio Molecular Dynamics Simulations. *Frontiers of Physics* **2018,** *13* (3), 1-7.

32. Kowalski, P. M.; Meyer, B.; Marx, D., Composition, Structure, And Stability Of The Rutile TiO_2 (110) Surface: Oxygen Depletion, Hydroxylation, Hydrogen Migration, And Water Adsorption. *Physical Review B* **2009,** *79* (11), 115410.

33. Samat, M.; Ali, A.; Taib, M.; Hassan, O.; Yahya, M., Hubbard U Calculations On Optical Properties Of 3d Transition Metal Oxide TiO_2. *Results In Physics* **2016,** *6*, 891-896.

34. Ziesche, P.; Kurth, S.; Perdew, J. P., Density Functionals From LDA to GGA. *Computational Materials Science* **1998,** *11* (2), 122-127.

35. Giese, T. J.; York, D. M., Density-Functional Expansion Methods: Evaluation Of LDA, GGA, And Meta-GGA Functionals And Different Integral Approximations. *The Journal of Chemical Physics* **2010,** *133* (24), 244107.

36. Himmetoglu, B.; Floris, A.; De Gironcoli, S.; Cococcioni, M., Hubbard-Corrected DFT Energy Functionals: The LDA+ U Description Of Correlated Systems. *International Journal of Quantum Chemistry* **2014,** *114* (1), 14-49.

37. Aryasetiawan, F.; Karlsson, K.; Jepsen, O.; Schönberger, U., Calculations of Hubbard U From First-Principles. *Physical Review B* **2006,** *74* (12), 125106.

38. Kulik, H. J.; Cococcioni, M.; Scherlis, D. A.; Marzari, N., Density Functional Theory In Transition-Metal Chemistry: A Self-Consistent Hubbard U Approach. *Physical Review Letters* **2006,** *97* (10), 103001.

39. Oba, F.; Choi, M.; Togo, A.; Tanaka, I., Point Defects In ZnO: An Approach From First Principles. *Science and Technology of Advanced Materials* **2011**.

40. Iwasawa, M.; Chen, Y.; Kaneta, Y.; Ohnuma, T.; Geng, H.-Y.; Kinoshita, M., First-Principles Calculation Of Point Defects In Uranium Dioxide. *Materials Transactions* **2006,** *47* (11), 2651-2657.

41. Becke, A. D., A New Mixing Of Hartree–Fock And Local Density-Functional Theories. *The Journal of Chemical Physics* **1993,** *98* (2), 1372-1377.

42. Zhang, I. Y.; Wu, J.; Xu, X., Extending The Reliability And Applicability Of B3LYP. *Chemical Communications* **2010,** *46* (18), 3057-3070.

43. Perdew, J. P.; Chevary, J. A.; Vosko, S. H.; Jackson, K. A.; Pederson, M. R.; Singh, D. J.; Fiolhais, C., Atoms, Molecules, Solids, And Surfaces: Applications Of The Generalized Gradient Approximation For Exchange And Correlation. *Physical Review B* **1992,** *46* (11), 6671.

44. Jensen, F., *Introduction To Computational Chemistry*. John wiley & sons: 2017.

45. Zhang, G.; Musgrave, C. B., Comparison Of DFT Methods For Molecular Orbital Eigenvalue Calculations. *The Journal Of Physical Chemistry A* **2007,** *111* (8), 1554-1561.

46. Tolba, S. A.; Gameel, K. M.; Ali, B. A.; Almossalami, H. A.; Allam, N. K., The DFT+ U: Approaches, Accuracy, And Applications. *Density Functional Calculations-Recent Progresses of Theory and Application* **2018**, 3-30.

47. Moynihan, G.; Teobaldi, G.; O'Regan, D. D., Inapplicability Of Exact Constraints And A Minimal Two-Parameter Generalization To The DFT+ U Based Correction Of Self-Interaction Error. *Physical Review B* **2016,** *94* (22), 220104.

48. Albers, R.; Christensen, N. E.; Svane, A., Hubbard-U Band-Structure Methods. *Journal of Physics: Condensed Matter* **2009,** *21* (34), 343201.

49. Ganduglia-Pirovano, M. V.; Hofmann, A.; Sauer, J., Oxygen Vacancies In Transition Metal And Rare Earth Oxides: Current State Of Understanding And Remaining Challenges. *Surface Science Reports* **2007,** *62* (6), 219-270.

50. Shi, H.; Liu, Y.-C.; Zhao, Z.-J.; Miao, M.; Wu, T.; Wang, Q., Reactivity Of The Defective Rutile TiO_2 (110) Surfaces With Two Bridging-Oxygen Vacancies: Water Molecule As A Probe. *The Journal of Physical Chemistry C* **2014,** *118* (35), 20257-20263.

51. Kremer, M. K.; Forrer, D.; Rogero, C.; Floreano, L.; Vittadini, A., Digging Ti interstitials at the r-TiO_2 (1 1 0) surface: Mechanism of porphyrin Ti sequestration by iminic N nucleophilic attack. *Applied Surface Science* **2021,** *564*, 150403.

52. Kresse, G.; Furthmüller, J., Efficiency Of Ab-Initio Total Energy Calculations For Metals And Semiconductors Using A Plane-Wave Basis Set. *Computational Materials Science* **1996,** *6* (1), 15-50.

53. Kresse, G.; Hafner, J., Ab Initio Molecular Dynamics For Liquid Metals. *Physical Review B* **1993,** *47* (1), 558.

54. Kresse, G.; Furthmüller, J.; Hafner, J., Theory Of The Crystal Structures Of Selenium And Tellurium: The Effect Of Generalized-Gradient Corrections To The Local-Density Approximation. *Physical Review B* **1994,** *50* (18), 13181.

55. Blöchl, P. E., Projector Augmented-Wave Method. *Physical Review B* **1994,** *50* (24), 17953.

56. Perdew, J. P.; Burke, K.; Ernzerhof, M., Generalized Gradient Approximation Made Simple. *Physical Review Letters* **1996,** *77* (18), 3865.

57. Stukowski, A., Visualization And Analysis Of Atomistic Simulation Data With OVITO–The Open Visualization Tool. *Modelling And Simulation In Materials Science And Engineering* **2009,** *18* (1), 015012.

58. Elliott, S. D.; Greer, J. C., Simulating the atomic layer deposition of alumina from first principles. *Journal of Materials Chemistry* **2004,** *14* (21), 3246-3250.

59. Gakis, G. P.; Vergnes, H.; Scheid, E.; Vahlas, C.; Boudouvis, A. G.; Caussat, B., Detailed investigation of the surface mechanisms and their interplay with transport phenomena in alumina atomic layer deposition from TMA and water. *Chemical Engineering Science* **2019,** *195*, 399-412.

60. Lownsbury, J. M.; Gladden, J. A.; Campbell, C. T.; Kim, I. S.; Martinson, A. B., Direct Measurements Of Half-Cycle Reaction Heats During Atomic Layer Deposition By Calorimetry. *Chemistry of Materials* **2017,** *29* (20), 8566-8577.

61. Rogala, M.; Bihlmayer, G.; Dabrowski, P.; Rodenbücher, C.; Wrana, D.; Krok, F.; Klusek, Z.; Szot, K., Self-Reduction Of The Native TiO_2 (110) Surface During Cooling After Thermal Annealing–In-Operando Investigation. *Scientific Reports* **2019,** *9* (1), 1-9.

62. Szot, K.; Rogala, M.; Speier, W.; Klusek, Z.; Besmehn, A.; Waser, R., TiO_2—A Prototypical Memristive Material. *Nanotechnology* **2011,** *22* (25), 254001.

63. Cho, W.; Sung, K.; An, K.-S.; Sook Lee, S.; Chung, T.-M.; Kim, Y., Atomic Layer Deposition Of Al2O3 Thin Films Using Dimethylaluminum Isopropoxide And Water. *Journal of Vacuum Science & Technology A: Vacuum, Surfaces, and Films* **2003,** *21* (4), 1366-1370.

64. Ghosh, M. K.; Choi, C. H., Adsorption Reactions of Dimethylaluminum Isopropoxide and Water on the H/Si (100)-2× 1 Surface: Initial Reactions for Atomic Layer Deposition of Al_2O_3. *The Journal of Physical Chemistry B* **2006,** *110* (23), 11277-11283.

65. An, K.-S.; Cho, W.-T.; Sung, K.-W.; Lee, S.-S.; Kim, Y.-S., Preparation of Al2O3 Thin Films By Atomic Layer Deposition Using Dimethylaluminum Isopropoxide And Water And Their Reaction Mechanisms. *Bulletin of the Korean Chemical Society* **2003,** *24* (11), 1659-1663.

66. Puurunen, R. L.; Lindblad, M.; Root, A.; Krause, A. O. I., Successive Reactions Of Gaseous Trimethylaluminium And Ammonia On Porous Alumina. *Physical Chemistry Chemical Physics* **2001,** *3* (6), 1093-1102.

67. Puurunen, R. L.; Root, A.; Haukka, S.; Iiskola, E. I.; Lindblad, M.; Krause, A. O. I., IR And NMR Study Of The Chemisorption Of Ammonia On Trimethylaluminum-Modified Silica. *The Journal of Physical Chemistry B* **2000,** *104* (28), 6599-6609.

68. Yates, D. J.; Dembinski, G.; Kroll, W.; Elliott, J. J., Infrared Studies Of The Reactions Between Silica And Trimethylaluminum. *The Journal of Physical Chemistry* **1969,** *73* (4), 911-921.

TOC Graphic

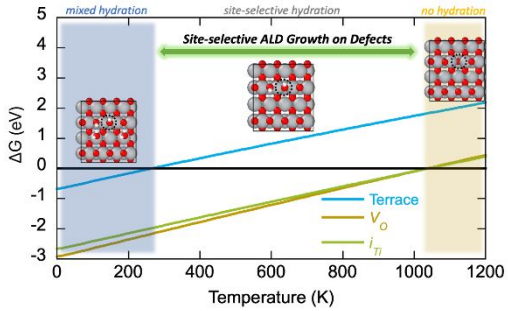
mixed hydration
site-selective hydration
no hydration
Site-selective ALD Growth on Defects
ΔG (eV)
Temperature (K)
Terrace
V_O
I_{Ti}